PAPER

Check for updates

Effective methods for the synthesis of hydrazones, quinazolines, and Schiff bases: reaction monitoring using a chemometric approach†

Jana Pisk, [ID] [a] Ivica Đilović, [ID] [a] Tomica Hrenar, [ID] [a] Danijela Cvijanović, [ID] [b] Gordana Pavlović[c] and Višnja Vrdoljak [ID] *[a]

Synthesis of hydrazones (**1a–4a** and **1b–4b**), quinazolines (**3c·MeOH** and **3d·MeOH**), and hydrazone-Schiff bases (**4c** and **4d**) is achieved by combining suitable aldehydes (2,3- or 2,4-dihydroxybenzaldehyde) with four hydrazides (isonicotinic, nicotinic, and 2- or 4-aminobenzoic acid hydrazide). A suite of approaches for their preparation is described: solution-based synthesis, mechanosynthesis, and solid-state melt reactions. The mechanochemical approach is generally a better choice for the quinazolines, while the solid-state melt reaction is more efficient for derivatives of (iso)nicotinic based hydrazones. Crystalline amine-functionalised hydrazones **4a** and **4b** undergo post-synthetic modifications in reactions with 3- or 4-pyridinecarbaldehyde vapours to form hydrazone-Schiff bases **4a-3py**, **4b-3py**, **4a-4py**, and **4b-4py**. Mechanochemical and vapour-mediated reactions are followed by *ex situ* powder X-ray diffraction and IR-ATR methods, respectively. The chemometric analysis of these data using principal component analysis provided an insight into the reaction profiles and reaction times. Azines (**5a** and **5b**), achieved from aldehydes and hydrazine, reversibly change colour in response to temperature changes. The structures of all products are ascertained by a combined use of spectroscopic and X-ray diffraction methods. The cytotoxic and antimicrobial activities of all compounds against selected human cancer cell lines and bacterial strains are evaluated.

Introduction

Hydrazide–hydrazones and quinazolin-4(3*H*)-ones are very attractive compounds in medicinal chemistry due to their broad spectrum of biological activities.[1–14] In particular, quinazolin-4(3*H*)-ones were reported to possess high anti-inflammatory and analgesic activity.[15] These properties have stimulated interest in developing methodologies for their synthesis. However, there is still an issue to find a simple and effective approach for their selective preparation.

The most common pathway for the preparation of these hydrazide-based compounds includes the reaction of appropriate hydrazides with different aldehydes or ketones in various organic solvents. Different solution-based synthetic approaches have been tested and combined.[16–19] Gudasi *et al.* described the ineffectiveness in synthesizing hydrazones by condensing pyridine-2-carbaldehyde with 2-aminobenzoylhydrazide.[17–19] It was found that reactions of the corresponding hydrazide and 3-methoxybenzaldehyde, in a molar ratio of 1 : 1, led to the formation of quinazolin-4(3*H*)-one. Recently, the mechano-chemical synthetic route provided an efficient solution for obtaining hydrazones[20] and 3-arylideneaminoquinazolin-4(1*H*)-one compounds, from various aldehydes.[21]

On account of it, 2,3- and 2,4-dihydroxybenzaldehyde were used as carbonyl forerunners, while isonicotinic and nicotinic

[a]University of Zagreb, Faculty of Science, Department of Chemistry, Horvatovac 102a, 10000 Zagreb, Croatia. E-mail: visnja.vrdoljak@chem.pmf.hr

[b]University of Zagreb, School of Medicine, Department of Chemistry and Biochemistry, Šalata 3, 10000 Zagreb, Croatia

[c]University of Zagreb, Faculty of Textile Technology, Division of Applied Chemistry, Prilaz baruna Filipovića 28a, 10000 Zagreb, Croatia

† Electronic supplementary information (ESI) available: (1) Analytical and spectral data, (2) view of structures and packing diagrams, (3) crystallographic data, and (4) powder diffraction patterns. Crystallographic data sets for the structures **1a·MeOH**, **1b·H₂O**, **3b**, **3c**, **4a**, **4b·MeOH**, **4c**, and **5b·H₂O**. CCDC 1985275–1985283. For ESI and crystallographic data in CIF or other electronic format see DOI: 10.1039/d0ra06845d
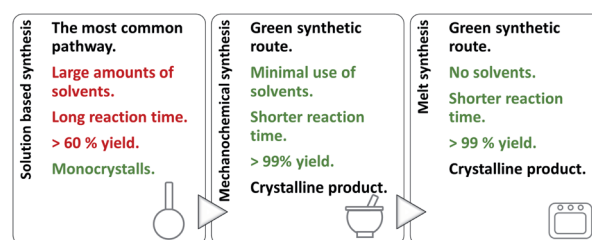

Fig. 1 Synthetic procedures applied for the preparation of hydra-zones, quinazolines, and hydrazine-Schiff bases.

acid hydrazides, were used as hydrazides for the hydrazones synthesis. Additionally, 2- and 4-aminobenzoic acid hydrazides were also investigated as compounds that provided classical hydrazones, quinazolinone or hydrazone-Schiff bases *via* controlled condensation. Conventional and a variety of green synthesis methodologies were used and critically compared (Fig. 1). We aimed to investigate their effect on reaction time, yield, as well as the crystallinity and purity of the prepared compounds. This study was also focused on applicability of the synthetic procedures and their selectivity towards the desired product. The synthetic path was refreshed by employing the "melt synthesis" technique.

Also, post-synthetic condensation with aldehyde vapours was applied to yield hydrazone-Schiff bases. The chemometric study was used for monitoring the starting material conversion by mechanochemical and vapour-mediated synthesis by processing *ex situ* powder X-ray diffraction and ATR spectra, respectively. Principal component analysis of these data was applied as a data reduction technique where collection of data (diffractograms or spectra) were decomposed in order to provide linearly independent variables. These variables can be plotted in one or two dimensions giving a detailed insight into reaction profiles and allowing identification of the reaction end points. Adequacy of the used method was validated by visual inspection of the final PXRD diffractograms and ATR spectra with the final product and in each case, it was confirmed that reaction finished in the exact time obtained by PCA.

Crystal and molecular structures of hydrazones **1a·MeOH**, **1b·H₂O**, **3a**, **3b**, **4a**, and **4b·MeOH**, quinazolinone **3c·MeOH**, hydrazone-Schiff base **4c**, and azine **5b·H₂O** were determined by the single crystal X-ray diffraction method, providing proposed investigation more comprehensive. It should be noted that in Cambridge Structural Database (CSD)[22] there are few hydrazone structures reported with 2,3- and 2,4-dihydroxybenzaldehyde fragment.[23–40] All of the investigated compounds were further characterized by elemental analysis, thermogravimetric and differential scanning calorimetry measurements, IR-ATR and NMR spectroscopy. The solid-state thermochromic changes of azines and influence of the central spacer and functional groups on the responsive properties were also explored.

To complement our study, the cytotoxicity of the compounds was evaluated against HepG2 and THP-1 cells. The compounds were also screened for their antimicrobial activity against *S. aureus*, *E. faecalis*, *E. coli* and *M. catarrhalis* to evaluate influence of the compound type and substituents on their activities.

Experimental section

General methods

Commercially available solvents were used without further purification. 2,3- and 2,4-dihydroxybenzaldehyde, isonicotinic and nicotinic acid hydrazide, and 2- and 4-aminobenzoic acid hydrazide, 3- and 4-pyridinecarboxaldehyde were used as received.

Elemental analyses were provided by the Analytical Services Laboratory of the Rudjer Bošković Institute, Zagreb, Croatia.

The powder X-ray diffraction data (PXRD) for qualitative phase analysis were collected on a Phillips X'Change powder diffractometer in the Bragg–Brentano geometry using CuK$_\alpha$ radiation. The data were collected and visualized using the X'Pert programs Suite.[41] IR-ATR spectra were recorded on a Perkin Elmer Spectrum One spectrometer. Thermogravimetric analyses (TGA) were conducted on a Mettler Toledo TG/DSC 3+ Stare System coupled with Thermo Fischer Nicolet iS50 FT-IR with Al₂O₃ crucibles under nitrogen stream in a temperature range between 25 °C and 400 °C, while the heating rate was adjusted to 10 °C min⁻¹. Differential scanning calorimetry (DSC) measurements were performed under the nitrogen stream on the Mettler-Toledo DSC823e calorimeter with aluminium crucibles, in the temperature range 25–400 °C, with the heating rate 10 °C min⁻¹. The results of both TGA and DSC experiments were evaluated using the Mettler STARe 9.01 software. Nuclear magnetic resonance (NMR) spectra were recorded on a Bruker Avance III HD 400 spectrometer operating at 400 MHz. Compounds were dissolved in dmso-d_6 and measured in 5 mm NMR tubes at 298 K with TMS as an internal standard.

Single-crystal X-ray measurements and structure determinations

The crystals of compounds **1a·MeOH** and **4b·MeOH** were air-sensitive so the single crystal diffraction data were collected at 150 K. Diffraction intensity data were collected by ω-scans on an Oxford Diffraction Xcalibur 3 (all compounds except **4c** and **5b·H₂O**) using graphite-monochromated MoKα radiation ($\lambda = 0.71073$ Å) and on an Oxford Diffraction Nova (**4c** and **5b·H₂O**) using micro-focus sealed X-ray tube with CuKα radiation ($\lambda = 1.54184$ Å). The data were reduced using the CrysAlis[42] program package. A summary of general and crystallographic data parameters is presented in Table S1, see ESI†.

The structures were solved by direct methods using SHELXT.[43] The refinement procedure by full-matrix least-squares methods based on F^2 values against all reflections included anisotropic displacement parameters for all non-H atoms. The positions of H atoms each riding on carbon atoms were determined on stereochemical grounds. The positions of other H atoms were determined from the difference Fourier map but were refined using the riding model. In the asymmetric unit of **3c·MeOH**, the methanol molecule exhibits a two-site (57 : 43) disorder. The restraints on geometrical and displacement parameters (DFIX, DELU, SIMU and ISOR) were applied for that molecule. Refinements were performed using SHELXL-97. The SHELX programs operated within the Olex² v1.2 (ref. 44) suite. Geometrical calculations and molecular graphics were done with PLATON, MERCURY,[45] ORTEP,[46] PyMOL[47] and POV-Ray.[48]

Solution synthesis

Synthesis of 1a, 1b, 2a, and 2b. A mixture of 2,3- or 2,4-dihydroxybenzaldehyde (0.35 g, 2.5 mmol) and isonicotinic or nicotinic hydrazide (0.34 g, 2.5 mmol) in 50 mL of methanol was refluxed with continuous stirring for 3 h. The obtained solution was cooled and after several days colourless crystalline product **1a**, **1b**, **2a**, or **2b** was filtered and dried in a desiccator up to

a constant weight. Yield: 0.53 g, 83% (**1a**); 0.59 g, 92% (**1b**); 0.52 g, 81% (**2a**); and 0.55 g, 86% (**2b**). Upon recrystallization and slow evaporation isoniazid-based hydrazones were obtained as solvates **1a·MeOH** (from methanol) and **1b·H₂O** (from acetone). Analytical, DSC, IR. and NMR spectral data are given in the ESI, Tables S2 and S3.†

Synthesis of 3a, 3b, 4a, and 4b. 2,3- or 2,4-Dihydroxybenzaldehyde (0.35 g, 2.5 mmol) dissolved in 20 mL of methanol was added dropwise to a solution of 2- or 4-aminobenzhydrazide (0.80 g, 2.5 mmol in 40 mL of ethanol) under stirring at room temperature. The mixture was continuously stirred for 30 min and then gently heated at 40 °C for 2 h. The resulting product **4a** precipitated during heating the reaction mixture. In the case of hydrazones **3a**, **3b**, and **4b**, the obtained solution was concentrated under vacuum to one-quarter of its volume and left at room temperature for several days. The obtained colourless crystalline product was filtered and dried in a desiccator up to a constant weight. Yield: 0.31 g, 46% (**3a**); 0.36 g, 53% (**3b**); 0.55 g, 82% (**4a**); and 0.53 g, 78% (**4b**). Crystals of **4b·MeOH** were obtained if the methanolic solution was evaporated slowly. Analytical, DSC, IR. and NMR spectral data are given in the ESI, Tables S4 and S5.†

Synthesis of 3c·MeOH, 4c, and 4d. 2- or 4-Aminobenzhydrazide (0.80 g, 2.5 mmol) was added to a methanolic solution of 2,3-dihydroxybenzaldehyde (0.69 g, 5.0 mmol in 30 mL). The solution was refluxed for 3 h and then, in the case of **3c**, concentrated under vacuum to one-quarter of its volume and left at room temperature for several days. The obtained precipitate was filtered and dried. Yield: 0.74 g, 76% (**3c**). Colourless crystals of **3c·MeOH** were obtained upon recrystallization from methanol. The resulting products **4c** and **4d** precipitated during heating the reaction mixture. They were isolated from hot solutions, rinsed and dried. Yield: 0.89 g, 91% (**4c**, a dark red powder); 0.79 g, 81% (**4c**, a yellowish-orange powder). Analytical, DSC, IR. and NMR spectral data are given in the ESI, Tables S6 and S7.†

Synthesis of 5a and 5b. A solution of hydrazine monohydrate (0.062 mL, 1.25 mmol) was added to an ethanolic solution of 2,3- or 2,4-dihydroxybenzaldehyde (0.35 g, 2.5 mmol in 15 mL) and the resulting solution was heated at 55 °C for 2 h. It afforded a crystalline product which was filtered, washed with ethanol and dried. Yield: 0.29 g, 84% (**5a**, a beige powder); 0.29 g, 84% (**5b**, a yellow powder). Crystals of **5b·H₂O** were obtained upon recrystallization of **5b** from acetonitrile. Analytical, DSC, IR. and NMR spectral data are given in the ESI, Table S8.†

Mechanochemical synthesis

Synthesis of 1a, 2b, 3a, 3b, 4a, and 4b. Liquid assisted grinding (LAG) experiments were performed using a Retsch MM200 ball mill. 0.1500 g (1 mmol) of an appropriate dihydroxybenzaldehyde, 1 mmol of an appropriate hydrazide and 50 μL of methanol were placed with one 10 mm milling ball in a 10 mL Teflon jar. A sample of the powder obtained after 60 min, milled at 25 Hz, was immediately analysed by PXRD. No purification of the sample was performed.

Synthesis of 3c and 3d. 0.1500 g (1 mmol) of an appropriate dihydroxybenzaldehyde, 0.05 mmol of an appropriate hydrazide and 50 μL of methanol were used. A sample of the powder obtained after 60 min, milled at 25 Hz, was immediately analysed by PXRD. No purification of the sample was performed.

Melt synthesis

Synthesis of 1a, 2a, 1b, and 2b. A mixture of 2,3- or 2,4-dihydroxybenzaldehyde (0.035 g, 0.25 mmol) and isonicotinic or nicotinic hydrazide (0.034, 0.25 mmol) were placed in a glass tube with glass stopper. The tube was placed in Kugelror oven and heated for one hour at 110 °C for **1a** and **2a** and 140 °C for **1b** and **2b**. Afterwards, samples were analysed by PXRD. No purification of the sample was performed.

Reaction monitoring and chemometric data analysis

Mechanochemical synthesis of 1a, 2b, 3a, 3b, 4a, and 4b. The syntheses were performed several times by using the same experimental conditions (10 mL Teflon jar with one 10 mm milling ball) each time starting from the reagents and grinding liquid. Reactions were conducted at 25 Hz frequency and the time was set to 2.5 min, 5 min, 10 min, 20 min, 30 min, 40 min, or 1 h. Afterwards, each sample was immediately analysed *ex situ* by PXRD. The sample was contained on a Si sample holder, patterns were collected in the range of $2\theta = 5–50°$, and chemometric data analysis was performed.

Vapour-mediated synthesis of 4a-3py, 4b-3py, 4a-4py, and 4b-4py. The reactions were performed in several independent sets at 25 °C. 10 mL of 3- or 4-pyridinecarbaldehyde was left overnight in a beaker inside a desiccator. A sample of **4a** or **4b** (10 mg) was placed on a watch glass, which was then put into the desiccator saturated with 3- or 4-pyridinecarbaldehyde vapour. The sample of each set was taken out after a certain period: 2,5; 5; 10; 20 min, and then every 30 min, and was subsequently analysed *ex situ* by IR-ATR spectroscopy, and then principal component analysis (PCA) was performed. The exposure time necessary to afford hydrazone-Schiff bases was determined: **4a-3py** (100 min), **4b-3py** (90 min), **4a-4py** (70 min), or **4b-4py** (120 min).

Chemometric data analysis

Statistical numerical analyses were performed using the second-order tensor decomposition tool principal component analysis, PCA. In PCA, the data matrix with mean-centered columns X of rank r is decomposed as a sum of r matrices t_i-p_i^τ each one with rank 1.

$$X = \sum_{i=1}^{r} t_i p_i^\tau$$

In one case the data matrix X was composed of PXRD diffractograms whereas in the other the data matrix was composed of ATR spectra. PCA enables one to find the best linear projections for a high dimensional set of data in the least-squares sense. Scores t_i represent projections of the original points on the principal component (PC) direction and can be used for classification or building of probability distributions,[49] whereas loadings[56] represent the eigenvectors of data covariance (or correlation) matrix and can be used for the identification of variability among the data. The initial development of PCA goes

back to Beltrami[50] and Pearson,[51] whereas the name was introduced by Hotelling.[52] More details on PCA can be found in the literature.[53] Principal component analysis was used as a dimensionality reduction tool for a set of PXRD diffractograms and for a set of ATR spectra. In each cae PCA was performed using a NIPALS algorithm[54] implemented in our own program *moonee*.[55,56]

In vitro cytotoxic and antibacterial activity

The synthesized compounds were tested *in vitro* against human acute monocytic leukemia (THP-1, ATCC TIB-202) and hepatocellular carcinoma (HepG2, ATCC HB-8065) cells. The cells were grown as reported.[57] The cytotoxicity studies were performed according to the protocol described previously.[57] In brief, the cytotoxicity of the tested compounds was evaluated at concentrations ranging from 0.05 to 100 μmol L^{-1} (THP-1) or 0.80 to 100 μmol L^{-1} (HepG2). The cells were seeded in 96-well microplates and incubated overnight before they were treated with varying concentrations of the tested compounds. The viability of cells after the compound treatment was determined using the MTS assay.[58] IC$_{50}$ (the concentration of the compound required to decrease cell viability for 50%) values were calculated for all tested compounds from dose–response curves. All experiments were performed in duplicate.

In vitro antibacterial activity of the investigated compounds was evaluated against Gram-positive, namely *Staphylococcus aureus* (ATCC 13709) and *Enterococcus faecalis* (ATCC 29212), and Gram-negative, namely *Escherichia coli* (ECM 1556) and *Moraxella catarrhalis* (ATCC 23246), bacterial strains by broth microdilution according to the CLSI guidelines.[59] Details of the bacterial growth and the method used have been described previously.[57] Briefly, the bacteria were seeded in 96-well microplates and incubated overnight before they were treated with varying concentrations of the tested compounds. After the treatment, the lowest concentrations at which no bacterial growth was observed were determined by visual inspection and reported as minimum inhibitory concentration (MIC) values. All experiments were performed in duplicate.

Results and discussion

Reactions of aldehydes with hydrazides in the molar ratio 1 : 1 – synthesis and structural studies of hydrazones

Solution-based synthesis. Hydrazones **1a–4a** and **1b–4b** (Fig. 2) were prepared by the condensation reaction of an appropriate hydrazide (nicotinic or isonicotinic hydrazide, and 2- or 4-aminobenzhydrazide) and aldehyde (2,3- or 2,4-dihydroxybenzaldehyde), in a molar ratio of 1 : 1, in methanol or ethanol. In the case of 2- or 4-aminobenzhydrazide-based hydrazones the crucial step was maintaining the room temperature and dropwise addition of aldehyde. Products obtained in such a way were taken as reference compounds to those obtained under green reaction conditions. Solvates were isolated upon recrystallization from methanol (**1a·MeOH**, **3c·MeOH**, **3d·MeOH**, and **4b·MeOH**) or acetone (**1b·H$_2$O**).
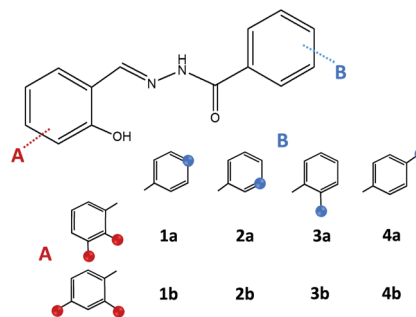

Fig. 2 Hydrazones **1a–4a** and **1b–4b**. Blue sphere presents N atom in the case of isonicotinic or nicotinic acid hydrazide, or NH$_2$ group in the case of 2- or 4-aminobenzoic acid hydrazide. Red sphere presents OH group.

Like in many similar compounds, the keto form dominates in the solid state (C=O bond is around 1.2 Å). An extensive survey of the Cambridge Structural Database shows that hydrazones derived from salicylaldehyde derivatives predominantly crystallize in the amide tautomeric form with *E*
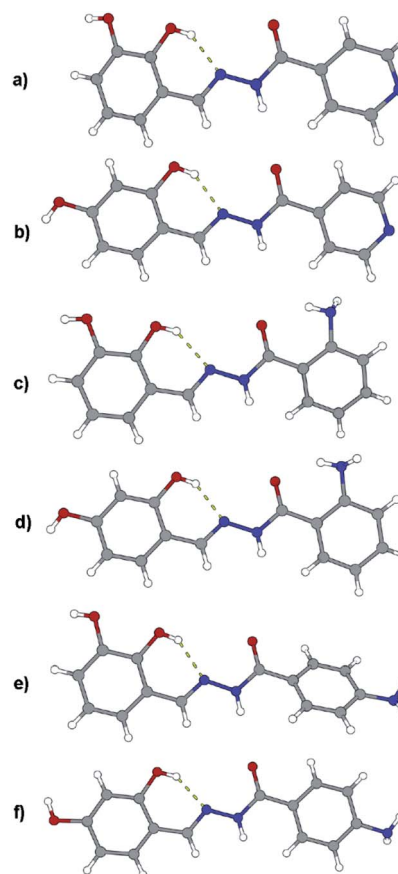

Fig. 3 Molecular structures of compounds: (a) **1a·MeOH**, (b) **1b·H$_2$O**, (c) **3a**, (d) **3b**, (e) **4a**, and (f) **4b·MeOH**. Solvent molecules were excluded because of clarity. Atoms are shown as spheres of arbitrary small radii. The intramolecular hydrogen bonds are indicated as an array of yellow cylinders. In all the structures carbonyl oxygen atom has label O1, neighboring nitrogen atoms N1 and N2 labels (the latter participates in intramolecular hydrogen bond).

configuration. This appears to be the case in all the investigated hydrazones (**1a·MeOH**, **1b·H₂O**, **3a**, **3b**, **4a**, and **4b·MeOH**): all of them have an intramolecular six-membered heteronuclear resonance-assisted hydrogen bond (Fig. 3). The *cis* configuration of the O1 atom with respect to N2 is present in all the examined molecules.

In all the crystal structures, molecules are almost planar or slightly inclined in a way to maximize their intermolecular hydrogen bonding potential (the planarity is disrupted in the case of solvated compounds). Planarity enhances the delocalization of π electrons through the spacer unit between two aromatic fragments, regardless of the position of substituents. This can be easily seen from the bond length distribution in the central parts of molecules (which fits well by already mentioned tautomeric form). The other, endocyclic, amino or hydroxyl, bond lengths and angles are comparable to those found in the CSD database for similar structures.

The crystal structures of the prepared hydrazones unveil that in all cases molecules are mutually connected with an extensive hydrogen bonding (Fig. 3, 4, 5, and S1–S6, see ESI†). The pyridine N atoms are connected with hydroxyl H atoms, carbonyl O atoms and amido H atoms are usually employed in hydrogen bonding with solvent molecules.

All solvates lose their solvent upon prolonged standing at room temperature. A comparison of PXRD patterns was used to identify obtained forms, Fig. S7, see ESI†. Structures of **1a** and **2a** were reported previously (CSD code WAFVEG and WOFYUN, respectively) but their synthesis was performed differently.[23,24]

Even-though a variety of products can be obtained by a solution-based method, large amounts of alcohol was employed. To minimize the use of solvent, and turn the synthetic protocols towards more sustainable ones: mechanochemical and solid-state melt-synthesis were engaged. The idea was to explore pros and cons of the methods as well as their selectivity towards the desired product.

Mechanochemical synthesis. By employing liquid assisted grinding (LAG), compounds **1a**, **2b**, **3a**, **3b**, **4a**, and **4b** were obtained in excellent yields (>99). All hydrazones prepared by the mechanochemical route had very similar PXRD patterns as the non-solvated ones prepared by the solution-based method (Fig. 6).
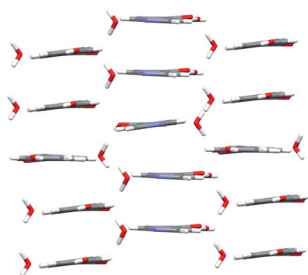

Fig. 5 Crystal packing of compound **4b·MeOH**. Molecules are connected with an extensive network of hydrogen bonds. Methanol molecules serve as a bridge between sheets of hydrazone molecules. The view is projected down the crystallographic *c* axis.

In the case of **1b** and **2a** longer milling was necessary which doesn't follow the sustainable conditions. Besides that, under the prolonged grinding the original PXRD patterns were found to be altered and the amorphization degree increased with milling time. Similarly, PXRD diffractograms of **1a**, **2b**, **3a**, **3b**, **4a**, and **4b** additionally milled for 30 min showed great amount of amorphous phase.

The first idea of the proposed research was to follow the formation of all hydrazones by *ex situ* PXRD and application of principal component analysis for the mechanochemical synthesis monitoring. PXRD were measured and collected in a data matrix *X* that was decomposed using the PCA. The duration of the milling was systematically increased up to 60 min to observe the influence of the milling duration on the

Fig. 4 Crystal packing of compound **1b·H₂O**. Molecules of **1b** are arranged in arrays which are mutually connected with hydrogen bonds (water molecules serve as a bridge) forming sheets. Sheets of molecules are held by stacking interactions and hydrogen bonds.
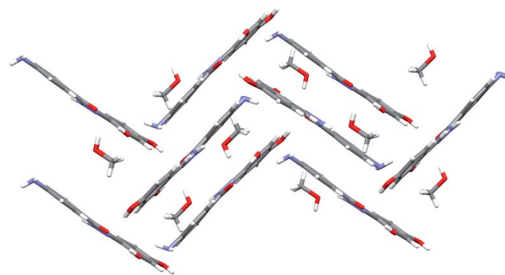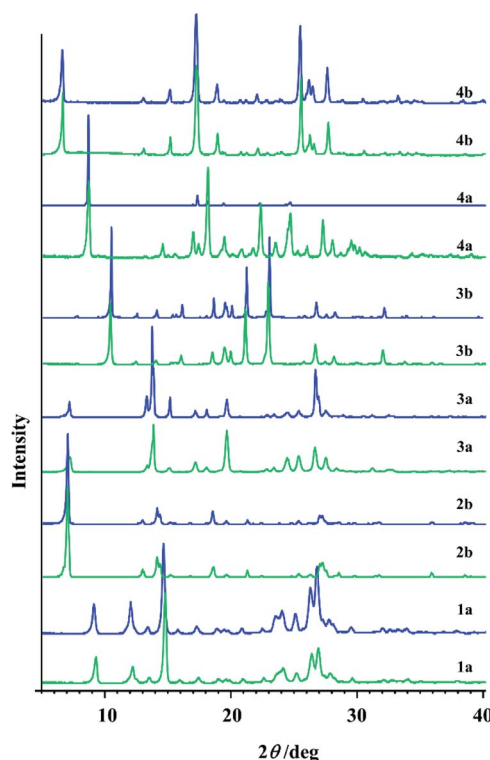

Fig. 6 PXRD patterns of hydrazones obtained by the solution-based method (blue line) and by the mechanosynthesis (green line).

reaction conversion. Even though it seemed that the PXRD patterns of the samples obtained after a particular reaction time fit well (Fig. S8, see ESI†), PCA revealed the problems in this kind of analysis for monitoring the reaction profiles and detection of reaction end.

Satisfactory results were not obtained in majority of cases due to the several causes: (a) mechanochemical reactions were too fast, (b) amorphization of the reaction components with milling time and reduction in overall quality of the data obtained, and (c) continuation of the reaction after the milling was stopped. In this way, after the reduction of data matrix composed of PXRD diffractograms and plotting the scores values in the dependence on time, the time scale on the ordinate was shifted by an unpredictable amount. This amount of time was different for each point in the reaction because the reaction was continued for different time.

Nevertheless, the PCA was able to provide some additional insight into the reaction mechanisms that we encountered and explained in our previous work.[57] For **4a** ligand the first principal component described only 41.56% of the total variance whereas the second described 27.57%. This low value of variance for the PC1 and relatively high value of variance for PC2 are indicators of many simultaneous reactions (at least two).[57] To confirm that fact, principal component loadings were plotted in 2- and 3-dimensional space and inspected visually. 2D and 3D loadings display a particular symmetrical "butterfly" pattern (Fig. 7a and b).[57]

This symmetrical pattern spanned along the first principal component (PC1) suggests that at least two orthogonal
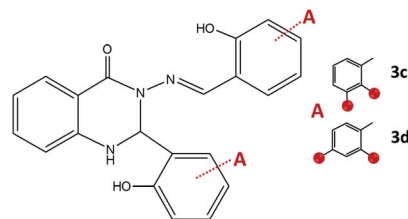
Fig. 8 2,3-Dihydroquinazolinones obtained by the reaction of 2-aminobenzhydrazide and 2,3-dihydroxybenzaldehyde, **3c**, and 2,4-dihydroxybenzaldehyde, **3d**. Red spheres present OH groups.

eigenvectors extracted from the original PXRD data are necessary for good description of the reaction profile. Since this arrangement is almost symmetrical along PC1 (with symmetry plane cutting the PC2-ordinate at 0.0) it is reasonable to expect that two or even more reactions are occurring simultaneously. To further confirm this fact, we investigated loadings in three dimensions (Fig. 7a). The pattern indeed looks two-dimensional where each branch of the loadings falls symmetrically on the side thus confirming two reaction steps.

Solid-state melt synthesis. Intrigued by the observed, we decided to explore whether the desired compounds could be reached in shorter reaction time by applying the solid-state melt reactions. For that purpose, the appropriate aldehyde and hydrazide, were placed in a glass tube and heated at the predetermined temperature (established according to the melting points of the used precursors and TG/DSC measurements, see ESI†). Hydrazones **1a**, **1b**, **2a**, and **2b** were easily obtained, and almost quantitative conversion was achieved (>99%). Samples obtained in such a way showed a higher amount of the crystalline phase in comparison to mechanochemically prepared samples. Although many materials are obtained by the melt-synthesis examples of hydrazones prepared by this technique, to the best of our knowledge, have not been reported so far.

However, 2- or 4-aminobenzhydrazide-based hydrazones were not accessible in this manner, and each time reactions gave a mixture of products. This suggests higher reactivity of the amino groups at the 2- and 4- position under these conditions.
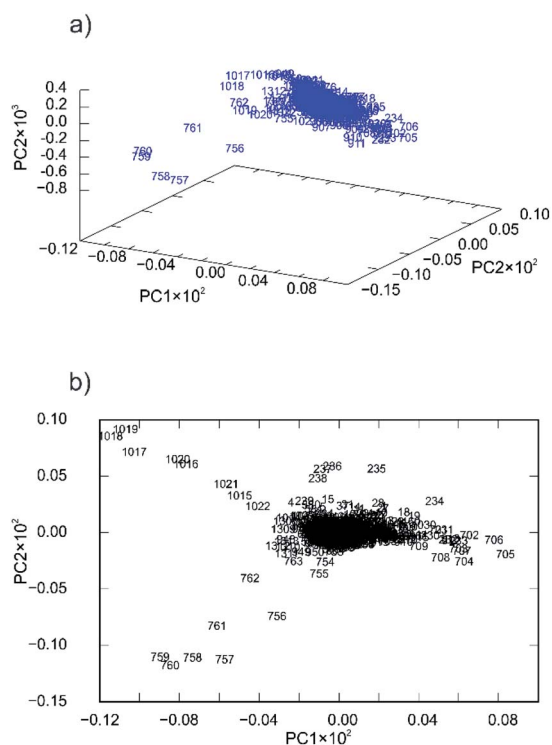

Fig. 7 Principal component loadings spanned by (a) three and (b) two principal components calculated for a set of PXRD data collected through mechanochemical synthesis of **4a**.

Reactions of aldehydes with hydrazides in the molar ratio 2 : 1 – synthesis and structural studies of quinazolines and hydrazone-Schiff bases

To explore a more profoundly variety of reaction routes, the synthesis was performed by changing the ratio of starting reagents (dihydroxybenzaldehydes and aminobenzhydrazides) to 2 : 1. The combination of 2-aminobenzhydrazide and 2,3-dihydroxybenzaldehyde in methanol gave crystals of **3c·MeOH**, Fig. 8. Formation of **3d** was not observed either under neutral conditions or in the presence of an acid, but instead, the 1 : 1 cyclic intermediate 3-amino-2-(2,4-dihydroxyphenyl)-4(3*H*)-quinazolinone (Scheme S1, see ESI†) was isolated from methanolic solution and characterized by NMR analysis. This result indicated that the reaction path was remarkably influenced by the position of the OH-group.
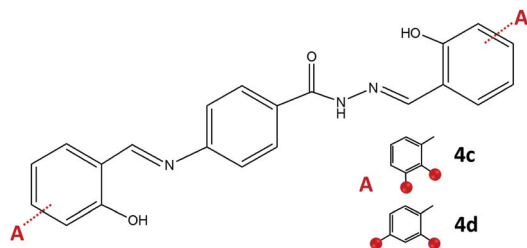
Fig. 9 Hydrazone–Schiff bases obtained by the reaction of 4-aminobenzhydrazide and 2,3-dihydroxybenzaldehyde, **4c**, and 2,4-dihydroxybenzaldehyde, **4d**. Red sphere presents OH group.

When employing 2-aminobenzhydrazide, the best results were obtained by using LAG mechanochemical method, and disubstituted quinazolin-4(3H)-one products **3c·MeOH** and **3d·MeOH** were prepared, Fig. 8. The heterocyclic product dominates in both cases, and purity of products was confirmed also by NMR analysis.

It seems, when 1 : 1 condensation product under solution-based or mechanochemical conditions was formed in the first step, the quinazoline product was not achieved in the next step even if 2,3- or 2,4-dihydroxysalicylaldehyde was added in excess (Scheme S1, see ESI†).

On the other hand, the condensation of 4-aminobenzhydrazide and 2,3- or 2,4-dihydroxybenzaldehyde provided hydrazone-Schiff bases **4c** and **4d** only by the solution-based method (Fig. 9). The LAG route did not afford pure compounds and according to NMR, a significant quantity of reagents remained post milling. Most probably hydrazone-Schiff base molecules assemble and afterwards disassemble under mechanical force.

Solutions of quinazolines and hydrazone-Schiff bases at room temperature were stable and no traces of the starting aldehydes, hydrazide or azine (vide infra) were detected as a result of the hydrolysis.[60] Their absence is proven by the XRD method.

Compound **3c** crystallizes as methanol solvate and its molecular structure contrasts the most among the other molecular structures. The reason emerges from the fact that during synthesis both terminal NH$_2$ groups were condensed with 2,3-dihydroxysalicylaldehyde. The resulting molecule consists of four cyclic fragments, out of four only one is heterocyclic and non-planar, Fig. 10. Since molecules crystallize in the centrosymmetric space group and sp^3 hybridized carbon atom is chiral, both stereoisomers can be found in the crystal structure. A relatively similar thing happened in the case with **4c** where two salicylaldehyde molecules condensed to both terminal NH$_2$ groups, Fig. 10. Molecules are mutually connected with an extensive hydrogen bonding (Fig. S9 and S10, see ESI†).

A comparison of reaction yields obtained by different approaches is given in Table 1. Besides high yields, the advantages of solid-state procedures also include operational simplicity and use of environmentally benign conditions.

Spectroscopic characterization

The IR-ATR spectra of all the compounds (except quinazolines **3c·MeOH** and **3d·MeOH**) confirmed the presence of the carbonyl group of the amide tautomer, indicated by sharp and intense absorption band in the range of 1680–1620 cm^{-1}. The corresponding band in **3c·MeOH** and **3d·MeOH** is overlapped with C=N band and due to it cannot be easily distinguished. All the compounds exhibited a vibration band at ca. 1610 cm^{-1} belonging to C=N$_{imine}$ group along with an absorption band at ca. 2850–2830 cm^{-1} attributed to C–H stretching of the –(C=O)–NH–N=CH– moiety. The band at ca. 1150 cm^{-1} is assigned to N–N stretching vibrations. Additionally, the spectra of solvates **3c·MeOH** and **3d·MeOH** showed the absorption band at around 1022 cm^{-1} implying the presence of the crystalline methanol.

The proton and carbon NMR chemical shifts of all compounds in dmso-d_6 solution were deduced by combined use of one (^{1}H, ^{13}C APT) and two-dimensional NMR techniques (COSY, HMQC and HMBC), Tables S2–S7 and Fig. S11–S22, in ESI.† The ^{1}H NMR spectra exhibited downfield singlet signals in
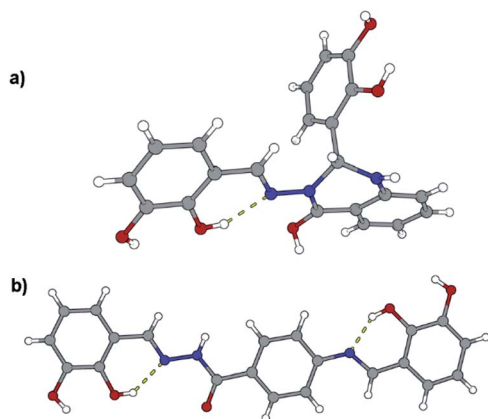

Fig. 10 Molecular structures of compounds: (a) **3c·MeOH** and (b) **4c**. Solvent molecules were excluded because of clarity. Atoms are shown as spheres of arbitrary small radii. The intramolecular hydrogen bonds are indicated as an array of yellow cylinders.

Table 1 Yields of synthesised products

Ligand	Synthetic procedure		
	Solution-based	Mechanochemistry	Melt synthesis
1a	83	>99	>99
1b	92	—	>99
2a	81	—	>99
2b	86	>99	>99
3a	46	>99	—
3b	53	>99	—
3c	76	>99	—
3d	—	>99	—
4a	82	>99	—
4b	78	>99	—
4c	91	—	—
4d	81	—	—

Table 2 Total variance represented by the first principal components calculated for a set of ATR data collected through mechanochemical syntheses
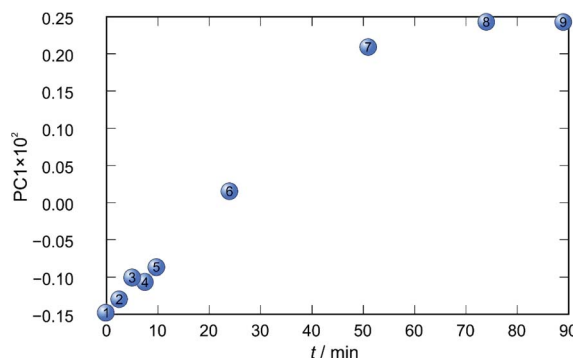
Component	4a-3py	4a-4py	4b-3py	4b-4py
PC1	76.62	86.42	92.65	74.58
PC2	15.08	8.08	4.47	16.03
PC3	3.33	2.82	1.26	4.62
PC4	2.04	1.40	0.70	3.36

the range from 9.11 to 13.32 ppm attributed to N=NH and phenolic OH protons, respectively. The broad OH and NH signals and chemical shift values indicated the presence of hydrogen-bonding interactions. The azomethine CH=N proton and carbon signals were observed in the range from 8.29 to 9.00 ppm and 149.39 to 165.64 ppm. In the ^{13}C NMR spectra, the low-field amide C=O carbon signals appeared in the range from 160.24 to 165.40 ppm.

Additionally, singlets observed around 6.4 ppm and 5.8 ppm were assigned to –NH$_2$ protons in the spectra of **3a–3b** and **4a–4b**, respectively. Quinazolines **3c** and **3d** showed the characteristic doublet peaks at 6.61 and 7.28 ppm, and 6.87 and 7.44 ppm, respectively in the ^{1}H NMR spectra. They were assigned to CH and NH protons of the quinazoline ring. The CH carbon atom of the quinazoline ring was observed around 66 ppm.

Vapour-mediated synthesis – yield optimization by a chemometric approach

Based on previously described results where 2 : 1 solution-based direct reaction provided the route to hydrazone-Schiff bases, we were interested to explore the possibility of altering hydrazones in the presence of aldehyde vapours. We exposed the crystals of synthesized aminobenzhydrazone-based derivatives **4a**, and **4b** to 3 or 4-pyridinecarboxaldehyde (**3py** or **4py**) vapours. After a certain period, the sample was taken out and was immediately analysed *ex situ* by IR-ATR spectroscopy. Long exposure time was necessary to complete the condensation reaction at 25 °C and to afford hydrazone-Schiff bases **4a-3py**,

Fig. 12 Time dependence of PC1 scores calculated for a set of IR-ATR data collected through a synthesis of **4a-4py**.

4b-3py, **4a-4py**, and **4b-4py**. It should be noted that these compounds could not be obtained pure in such manner from solution most probably due to the capacity of hydrazones to readily undergo transimination reaction.

Application of principal component analysis to IR-ATR spectral data obtained by reaction monitoring provided a detailed insight into the reaction profiles and the detection of reaction end. These profiles can be well represented using only the 1st principal component (Fig. 11–14).

In each case the PC1 describes more than 70% of the total variance (Table 2). These high values of explained variances in the principal component ensure the proper description of the reaction with only the first principal component. The first component picks up the most prominent changes during reactions. The reaction profiles nicely show the progress and the end of the reaction. For the vapour-mediated synthesis of **4a-3py** and **4a-4py** the end of the reaction can be estimated to be 100 and 90 min (Fig. 11 and 12), respectively. In the case of **4b-3py** and **4b-4py** these values were estimated to be 70 and 120 minutes (Fig. 13 and 14). These values were confirmed by comparison of the spectra measured in these times with the spectrum of final product. Loadings vectors for monitored reactions are presented on Fig. S23–S26.† Investigation of loadings vectors confirms the creation of products during reactions.
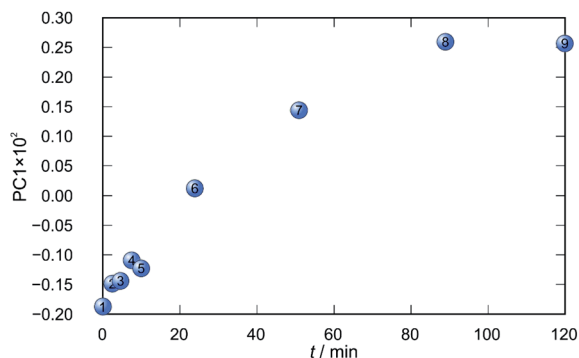
Fig. 11 Time dependence of PC1 scores calculated for a set of IR-ATR data collected through a synthesis of **4a-3py**.
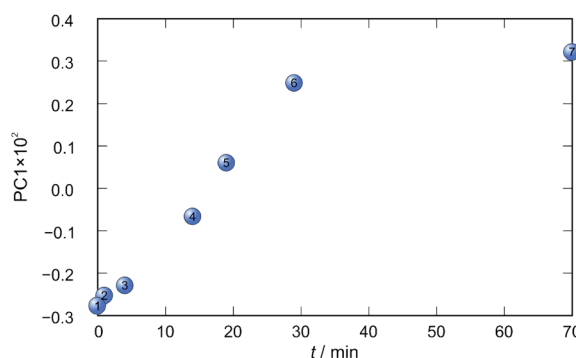
Fig. 13 Time dependence of PC1 scores calculated for a set of IR-ATR data collected through a synthesis of **4b-3py**.
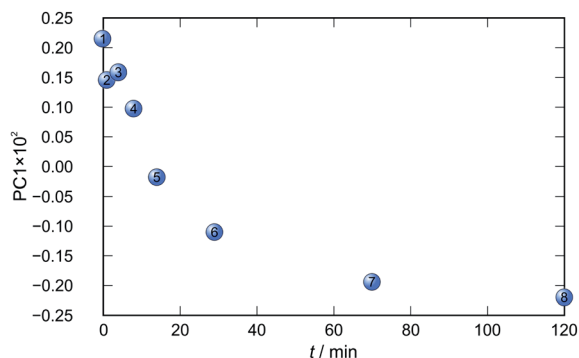
Fig. 14 Time dependence of PC1 scores calculated for a set of IR-ATR data collected through a synthesis of **4b-4py**.

Investigation of spectral patterns confirmed that reactions were completed in the time predicted by the PC1 reaction profiles. A comparison of the NMR spectra is given in Fig. S27, see ESI†. Singlets observed around 5.8 ppm, assigned to $-NH_2$ protons in the spectra of **4a** and **4b**, are missing in the spectra of the hydrazone-Schiff bases.

Reactions of aldehydes with hydrazine in the molar ratio 2 : 1 – synthesis of azines

To gain more insight into a variety of synthetic outcomes for the reactions carried out in the molar ratio of 2 : 1, hydrazine was used instead of hydrazides. The azine derivatives **5a** and **5b** (Fig. 15) were obtained by condensing 2,3- and 2,4-dihydroxybenzaldehyde with hydrazine, respectively (yield: 84%). Crystals of **5b·H₂O** were obtained upon crystallization from acetonitrile (Fig. 16). In **5b·H₂O** parallel sheets are mutually interconnected *via* water molecules (Fig. 17). NMR spectra with the NMR numbering scheme are given in Fig. S28–S30 and Table S8, see ESI†

Thermal behaviour

All compounds, except solvates, remained stable in the solid state for a longer time at RT. The azine **5b** demonstrated the largest thermal stability and the lowest one was detected for the quinazolines **3c** and **3d** (see ESI†). All compounds were analysed with TG-FTIR through heating the samples from 25 to 400 °C. It is seen that methanol is present in the structure of quinazolines **3c·MeOH** and **3d·MeOH**, confirming the previous assumption seen through IR-ATR.
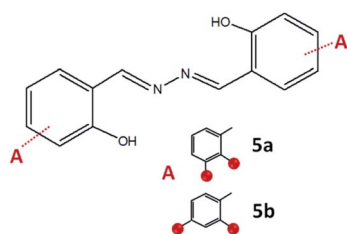

Fig. 15 Compounds obtained by the reaction of azine and 2,3-dihydroxybenzaldehyde, **5a**, and 2,4-dihydroxybenzaldehyde, **5b**. Red sphere presents OH group.
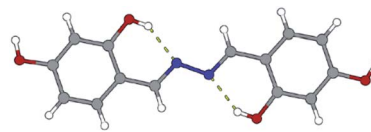

Fig. 16 Molecular structures of compound **5b·H₂O**. The solvent molecule was excluded because of clarity. Atoms are shown as spheres of arbitrary small radii. The intramolecular hydrogen bonds are indicated as an array of yellow dotted lines.

TG-FTIR analysis of compounds **4a–4d**, as well as **5a** and **5b**, indicates absorption bands characteristic for ammonia in the IR spectra during decomposition of the mentioned compounds caused by heating. On the other hand, the TG-FTIR spectra of the compounds **1a–3a** and **1b–3b** did not provide results that could be easily interpreted.

The solid-state thermochromic behaviour

Since hydrazone-Schiff bases are intensively coloured we aimed to investigate thermochromic behavior of all 2 : 1 compounds. Interestingly, pronounced solid-state thermochromic changes in the solid state were observed only for azine **5a**. The beige crystals of **5a**, were found to turn orange-red when heated slowly above room temperature up to 225 °C (Fig. 18). The initial colour reverted on cooling to room temperature. The gradual colour changes were observed repeatedly on heating and subsequent cooling.

To elucidate the thermal behaviour of **5a**, several series of cyclic DCS experiments were conducted. The thermograms, during several heating runs from 25 °C to 225 °C, did not exhibit any peaks and therefore phase transformations could be excluded. It is, therefore, reasonable to assume that the gradual colour changes could be caused by changes in the intermolecular interactions.[61]

In all crystal structures, molecules are almost planar, and a similar scenario could be assumed also for **5a**. We assume that at higher temperatures, the increased unit cell volume and the distance between assembled molecules could influence the charge delocalization.

The colour change of **5b·H₂O** upon heating up to 300 °C was less pronounced (from yellow to light orange). This is most probably influenced by the distance between molecules in the crystal structure. Thermochromic changes were not observed for hydrazone-Schiff bases, implying the importance of the aldazine –C=N–N=C– unit towards the external stimuli.
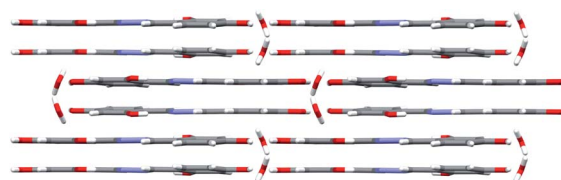

Fig. 17 Crystal packing of compound **5b·H₂O**. Molecules are connected with an extensive network of hydrogen bonds. Parallel sheets are mutually interconnected *via* water molecules. The view is projected down the crystallographic *c* axis.
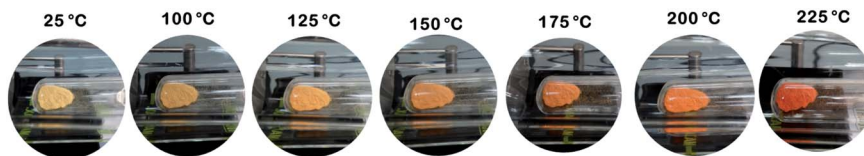
Fig. 18 The solid–state thermochromic behaviour of **5a**. The images of the temperature effects on the appearance of azine **5a** were taken when sample was heated in Kugelror oven. The beige colour is recovered after it was cooled to room temperature.

In vitro cytotoxic and antibacterial activity

The results obtained by the MTS assay are given in Table S9, see ESI†. Due to the IC$_{50}$ values higher than 100 μmol L^{-1}, all the tested compounds can be considered noncytotoxic against HepG2 cells. Only compounds **3c** and **4d** with the IC$_{50}$ values of 69.18 and 22.46 μmol L^{-1} can be considered somewhat cytotoxic against THP-1 cells. No cytotoxic effect on HepG2 cells had also been established for the related aroylhydrazones derived from salicylaldehyde, 3- or 4-methoxysalicylaldehyde.[57,62]

Unlike the tested hydrazones (**1a–4a** and **1b–4b**), these related hydrazones had been reported to exhibit weak to moderate cytotoxicity against THP-1 cells.[57,62] Several observations can be highlighted about the factors affecting the cytotoxic activity of hydrazones on THP-1 cells. To specify, introducing the hydroxy group on position 3- and 4- of the salicylaldehyde moiety significantly lowered the cytotoxic activity. Replacing the 3- or 4-methoxy group by a hydroxy one also decreased the hydrazone cytotoxicity. In addition, the cytotoxicity of hydrazones diminished upon introduction of nitrogen into the benzhydrazide moiety regardless of whether the nitrogen is a part of the ring or the amino group.

In general, as seen from the high MIC values (Table S10, see ESI†), the investigated compounds did not inhibit the growth of Gram-positive bacteria. Regarding the Gram-negative bacteria, the majority of tested compounds (excluding the azines) exhibited a weak growth-inhibitory effect on *E. coli* while most of them showed moderate antibacterial activity against *M. catarrhalis*. However, the observed activity of the tested compounds on *M. catarrhalis* was substantially lower compared to the reference antibiotic azithromycin.

The only hydrazone that exhibited broad-spectrum activity was **2a**. Interestingly, hydrazone **2b** that differs from **2a** only in the position of a hydroxy group was found to be inactive against all selected bacterial strains. The influence of the hydroxy group position on the anti-*M. catarrhalis* activity observed in hydrazones derived from isonicotinic, 2- or 4-aminobenzoic acid hydrazide is not as pronounced as in hydrazones **2a** and **2b**. Specifically, the anti-*M. catarrhalis* activity of **4a** is four times greater than the activity of **4b** while the MIC values for **1a** and **1b** as well as for **3a** and **3b** differ even less. Also, a slightly greater inhibitory effect of 4- over 3-hydroxy isomer was observed only for 2-aminobenzoylhydrazones (**3a** and **3b**).

The higher antibacterial activity against Gram-negative bacteria of the 3-hydroxy isomer, when compared to the corresponding 4-hydroxy isomer, was established not only for hydrazones but also for all other investigated types of compounds. Moreover, the azine containing the 3-hydroxy groups (**5a**) was one of the most efficient tested compounds while the azine with 4-hydroxy groups (**5b**) did not inhibit the growth of *M. catarrhalis* (Table S9†).

Quinazolinones **3c** and **3d** and Schiff bases **4c** and **4d**, were generally more active against *M. catarrhalis* than the corresponding hydrazones (**3a**, **3b**, **4a**, and **4b**, respectively).

Conclusions

The results described in this paper demonstrate that a specific condensation reaction can take place preferentially by using different green synthetic methodologies. The use of mechanochemical synthesis is beneficial in terms of ease of work-up and high yields, in comparison to solution-based synthesis. It also represents a preferable synthetic procedure for obtaining 4(3*H*)-quinazolinone core products. But in the case of the hydrazones, it has a limited application. Nevertheless, the solid-state melt reaction offers an easy pathway to obtain hydrazones that cannot undergo further condensation reactions. However, in order to analyse the molecular and crystal structures, solution-based methods are still beneficial.

Mild reaction conditions are necessary for the post-synthetic modification of 4-aminobenzhydrazones. Furthermore, vapour-mediated synthesis is the superior approach to convert the primary amine group into an imine functionality and to avoid transimination processes.

Mechanochemical and vapour-mediated reactions can be successfully followed by *ex situ* PXRD and IR-ATR methods thus avoiding the use of a solution-phase spectroscopic analysis and possibility of further reaction occurrence. Implementation of principal component analysis provided a detailed insight into the reaction profiles and detection of reaction end.

The azines exhibited temperature-responsive colour change. The central unit and position of functional groups in molecules affects their response.

Quinazolinones and Schiff bases are generally more active against *M. catarrhalis* than the corresponding hydrazones. Introducing the hydroxy group on position 3- and 4- of the salicylaldehyde moiety significantly lowered the cytotoxic activity.

Conflicts of interest

There are no conflicts of interest to declare.

Acknowledgements

Notes and references

1 D. Kumar, N. Maruthi Kumar, S. Ghosh and K. Shah, *Bioorg. Med. Chem. Lett.*, 2012, **22**, 212–215.

2 B. Yadagiri, U. D. Holagunda, R. Bantu, L. Nagarapu, V. Guguloth, S. Polepally and N. Jain, *Bioorg. Med. Chem. Lett.*, 2014, **24**, 5041–5044.

3 S. S. Machakanur, B. R. Patil, D. S. Badiger, R. P. Bakale, K. B. Gudasi and S. W. A. Bligh, *J. Mol. Struct.*, 2012, **1011**, 121–127.

4 T. Nasr, S. Bondock and M. Youns, *Eur. J. Med. Chem.*, 2014, **76**, 539–548.

5 K. Vasantha, G. Basavarajaswamy, M. Vaishali Rai, P. Boja, V. R. Pai, N. Shruthi and M. Bhat, *Bioorg. Med. Chem. Lett.*, 2015, **25**, 1420–1426.

6 B. Çakır, Ö. Dağ, E. Yıldırım, K. Erol and M. F. Şahin, *J. Fac. Pharm. Gazi.*, 2001, **18**, 99–106.

7 S. Şenkardeş, N. Kaushik-Basu, İ. Durmaz, D. Manvar, A. Basu, R. Atalay and Ş. G. Küçükgüzel, *Eur. J. Med. Chem.*, 2016, **108**, 301–308.

8 A. Inam, S. M. Siddiqui, T. S. Macedo, D. R. M. Moreira, A. C. L. Leite, M. B. P. Soares and A. Azam, *Eur. J. Med. Chem.*, 2014, **75**, 67–76.

9 R. J. Butcher, J. P. Jasinski, B. Narayana, K. Sunil and H. S. Yathirajan, *Acta Crystallogr., Sect. E: Struct. Rep. Online*, 2007, **63**, o4025–o4026.

10 A. Mandal and B. K. Patel, *J. Mol. Struct.*, 2018, **1155**, 78–89.

11 X.-S. Wang, J. Sheng, L. Lu, K. Yang and Y.-L. Li, *ACS Comb. Sci.*, 2011, **13**, 196–199.

12 M. Ikram, S. Rehman, F. Subhan, M. N. Akhtar and M. O. Sinnokrot, *Open Chem.*, 2017, **15**, 308–319.

13 D. Tinguiano, A. Sy, I. E. Thiam, M. Gaye and P. Retailleau, *Acta Crystallogr., Sect. E: Struct. Rep. Online*, 2012, **68**, o2374–o2375.

14 K. B. Gudasi, S. A. Patil, R. S. Vadavi, R. V. Shenoy and M. Nethaji, *Transition Met. Chem.*, 2006, **31**, 586–592.

15 A. C. Tinker, H. G. Beaton, N. Boughton-Smith, S. L. Cooper, L. Fraser-Rae, K. Hallam, P. Hamley, T. McInally, D. J. Nicholls, A. D. Pimm and A. V. Wallace, *J. Med. Chem.*, 2003, **46**, 913–916.

16 F. Fülöp, M. F. Simeonov and K. Pihlaja, *Tetrahedron*, 1992, **48**, 531–538.

17 K. B. Gudasi, R. S. Vadavi, R. V. Shenoy, S. A. Patil and M. Nethaji, *Transition Met. Chem.*, 2006, **31**, 374–381.

18 K. B. Gudasi, R. S. Vadavi, R. V. Shenoy, S. A. Patil and M. Nethaji, *Transition Met. Chem.*, 2006, **31**, 135–145.

19 R. S. Hunoor, B. R. Patil, D. S. Badiger, R. S. Vadavi, K. B. Gudasi, C. V. Magannavar and I. S. Muchand, *Chem. Pharm. Bull.*, 2010, **58**, 712–716.

20 P. F. M. Oliviera, M. Baron, A. Chamayou, C. André-Barrès, B. Giidetti and M. Baltas, *RSC Adv.*, 2014, **4**, 56736.

21 S. Kuntikana, C. Bhat, M. Kongot, S. I. Bhat and A. Kumar, *ChemistrySelect*, 2016, **1**, 1723–1728.

22 F. H. Allen, *Acta Crystallogr. B*, 2002, **58**, 380, The Cambridge Structural Database, V5.30.

23 E. Tecer, N. Dege, A. Zülfikaroğlu, N. Senyüz and H. Batı, *Acta Crystallogr., Sect. E: Struct. Rep. Online*, 2010, **66**, o3369–o3370.

24 N. Dege, N. Senyüz, H. Batı, N. Günay, D. Avcı, Ö. Tamer and Y. Atalay, *Spectrochim. Acta, Part A*, 2014, **120**, 323–331.

25 D. Sadhukhan, M. Maiti, G. Pilet, A. Bauzá, A. Frontera and S. Mitra, *Eur. J. Inorg. Chem.*, 2015, 1958–1972.

26 M. Taha, M. S. Baharudin, N. H. Ismail, S. A. Shah and S. Yousuf, *Acta Crystallogr., Sect. E: Struct. Rep. Online*, 2012, **68**, o3256.

27 M. Sutradhar, E. C. B. A. Alegria, K. T. Mahmudov, M. F. C. Guedes da Silva and A. J. L. Pombeiro, *RSC Adv.*, 2016, **6**, 8079–8088.

28 H. M. Ali, S. Puvaneswary, W. J. Basirun and S. W. Ng, *Acta Crystallogr., Sect. E: Struct. Rep. Online*, 2005, **61**, o1013–o1014.

29 H. M. Ali, S. Puvaneswary, W. J. Basirun and S. W. Ng, *Acta Crystallogr., Sect. E: Struct. Rep. Online*, 2005, **61**, o1083–o1084.

30 M. Albrecht, I. Latorre, Y. Liu and R. Fröhlich, *Z. Naturforsch., B: J. Chem. Sci.*, 2010, **65**, 311–316.

31 P. Promdet, J. Horkaew, S. Chantrapromma and H.-K. Fun, *Acta Crystallogr., Sect. E: Struct. Rep. Online*, 2011, **67**, o3224.

32 Y.-M. Chen, Q.-R. Zeng, Y. Li, J.-N. Lin, J.-M. Wang, B. Qu and Q.-F. Xie, *Chin. J. Inorg. Chem.*, 2016, 1398–1404.

33 M. Mohanraj, G. Ayyannan, G. Raja and C. Jayabalakrishnan, *Mater. Sci. Eng. C*, 2016, **69**, 1297–1306.

34 C. Arunagiri, A. G. Anitha, A. Subashini and S. Selvakumar, *J. Mol. Struct.*, 2018, **1163**, 368–378.

35 M. Taha, N. H. Ismail, H. M. Zaki, A. Wadood, E. H. Anouar, S. Imran, B. M. Yamin, F. Rahim, M. Ali and K. M. Khan, *Bioorg. Chem.*, 2017, **75**, 235–241.

36 N. M. Lair, H. Khaledi and H. M. Ali, *Acta Crystallogr., Sect. E: Struct. Rep. Online*, 2011, **67**, o459.

37 M. Sánchez-Lozano, E. M. Vázquez-López, J. M. Hermida-Ramón and C. M. Estévez, *Polyhedron*, 2011, **30**, 953–962.

38 J. D. Siqueira, A. C. O. Menegatti, H. Terenzi, M. B. Pereira, D. Roman, E. F. Rosso, P. C. Piquini, B. A. Iglesias and D. F. Back, *Polyhedron*, 2017, **130**, 184–194.

39 H. S. Naveenkumar, A. Sadikun, P. Ibrahim, W.-S. Loh and H.-K. Fun, *Acta Crystallogr., Sect. E: Struct. Rep. Online*, 2010, **66**, o1202–o1203.

40 Z. Wei, J. Wang, X. Jiang, Y. Li, G. Chen and Q. Xie, *Chin. J. Appl. Chem.*, 2015, **32**, 1014–1021.

41 *X'Pert Software Suite, Version 1.3e*, Panalytical B. V., Almelo, The Netherlands, 2001.

42 *CrysAlis Software system, Version 1.171.33.32*, Xcalibur CCD system, Oxford Diffraction Ltd, Abingdon, UK, 2009.

43 G. M. Sheldrick, *Acta Crystallogr. A*, 2008, **64**, 112–122.

44 O. V. Dolomanov, L. J. Bourhis, R. J. Gildea, J. A. K. Howard and H. Puschmann, *J. Appl. Cryst.*, 2009, **42**, 339–341.

45 C. F. Macrae, P. R. Edgington, P. McCabe, E. Pidcock, G. P. Shields, R. Taylor, M. Towler and J. van de Streek, *J. Appl. Cryst.*, 2006, **39**, 453–457.

46 L. J. Farrugia, *J. Appl. Crystallogr.*, 1997, **30**, 565.

47 *The PyMOL Molecular Graphics System, Version 1.2r3pre*, Schrödinger, LLC.

48 http://www.povray.org/.

49 T. Hrenar, I. Primožič, D. Fijan and M. Majerić Elenkov, *Phys. Chem. Chem. Phys.*, 2017, **19**, 31706–31713.

50 E. Beltrami, *Giornale di Matematiche ad Uso degli Studenti Delle Università*, 1873, vol. 11, pp. 98–106.

51 K. Pearson, *Philos. Mag.*, 1901, **2**, 559–572.

52 H. Hotelling, *J. Educ. Psychol.*, 1933, **24**, 417–441.

53 I. T. Jolliffe, *Principal Component Analysis*, Springer, Berlin, 1986.

54 P. Geladi and B. Kowalski, *Anal. Chim. Acta*, 1986, **185**, 1–17.

55 T. Hrenar, *moonee, Program for Manipulation and Analysis of Multi- and Univariate Data, rev. 0.6827*, 2017.

56 O. Jović, T. Smolić, I. Primožič and T. Hrenar, *Anal. Chem.*, 2016, **88**, 4516–4524.

57 J. Pisk, T. Hrenar, M. Rubčić, G. Pavlović, V. Damjanović, J. Lovrić, M. Cindrić and V. Vrdoljak, *CrystEngComm*, 2018, **20**, 1804–1817.

58 T. Mosmann, *J. Immunol. Methods*, 1983, **65**, 55–63.

59 CLSI, Methods for Dilution Antimicrobial Susceptibility Tests for Bacteria that Grow Aerobically; Approved Standard-Eight edition, *CLSI document M07-A8*, Clinical and Laboratory Standards Institute, Wayne, USA, 2009.

60 V. Vrdoljak, B. Prugovečki, I. Primožič, T. Hrenar, D. Cvijanović, J. Parlov Vuković, R. Odžak, M. Skočibušić, S. Prugovečki, J. Lovrić, D. Matković-Čalogović and M. Cindrić, *New J. Chem.*, 2018, **42**, 11697–11707.

61 P. Naumov, S. C. Lee, N. Ishizawa, Y. G. Jeong, I. H. Chung and S. Fukuzumi, *J. Phys. Chem. A*, 2009, **113**, 11354–11366.

62 M. Cindrić, A. Bjelopetrović, G. Pavlović, V. Damjanović, J. Lovrić, D. Matković-Čalogović and V. Vrdoljak, *New J. Chem.*, 2017, **41**, 2425–2435.